On the Equivalence of Brownian Dynamics and Dynamic Monte Carlo Simulations in Multicomponent Colloidal Suspensions

Alejandro Cuetos[1] and Alessandro Patti[2,*]
[1] *Department of Physical, Chemical and Natural Systems, Universidad Pablo Olavide, 41013 Sevilla, Spain*
[2] *School of Chemical Engineering and Analytical Science, The University of Manchester, Sackville Street, Manchester M13 9PL, UK*

We propose a simple, but powerful theoretical framework to quantitatively compare Brownian dynamics (BD) and dynamic Monte Carlo (DMC) simulations of multicomponent colloidal suspensions. By extending our previous study focusing on monodisperse systems of rod-like colloids, here we generalize the formalism described there to multicomponent colloidal mixtures and validate it by investigating the dynamics in isotropic and liquid crystalline phases containing spherical and rod-like particles. In order to investigate the dynamics of multicomponent colloidal systems by DMC simulations, it is key to determine the elementary timestep of each species and establish a unique time scale. This is crucial to consistently study the dynamics of colloidal particles with different geometry. By analyzing the mean square displacement, the orientation auto-correlation functions and the self part of the van Hove correlation functions, we show for the first time that DMC simulation is a very convenient and reliable technique to describe the stochastic dynamics of any multicomponent colloidal system. Our theoretical formalism can be easily extended to any colloidal system containing size and/or shape polydisperse particles.

PACS numbers: 82.70.Dd, 61.30.-v, 87.15.Vv

A. Introduction

Colloids consist of supramolecular nanoparticles evenly dispersed in a fluid, usually a liquid. While the prefix *nano* indicates that these particles have at least one of their dimensions in the submicrometer range, the term *supramolecular* stresses that their characteristic length scale, typically between 10 nm and 10 μm, is significantly larger than that of conventional molecules [1]. Due to their relatively small size, the dynamics of colloidal particles is substantially controlled by the stochastic collisions with the surrounding molecules of the solvent and is usually referred to as Brownian motion. This random drifting stems from a thermal energy of the order of k_BT per particle, with k_B the Boltzmann's constant and T the absolute temperature. In order to keep the particles dispersed in the medium and prevent their sedimentation, the thermal energy should be larger than the gravitational potential energy. Equivalently, the particles' radius R should be smaller than the sedimentation length $\lambda_{sed} = k_BT/m_bg$, with g the gravitational acceleration and m_b the buoyant mass [2].

Understanding the dynamical behavior and rheological properties of colloidal suspensions is one of the cutting-edge themes of the current research in material science. The fundamental problems involved, such as rheology under external fields and crystallization, have a crucial impact on the formulation of several products, including paints, pharmaceutical creams, foods, and inks. For example, paints are expected to flow easily upon application on a vertical surface, but should not flow by their own weight. Dense colloidal suspensions can display an abrupt increment in viscosity when an increasing shear stress is applied [3]. On the one hand, this shear thickening can deeply alter the structural properties of the suspension and hence compromise the correct functioning of the processing equipment. On the other hand, this behavior is very convenient, for instance, for the oil and gas industry to protect a well from blowouts, usually observed when a drill reaches a gas pocket and provokes a sudden release of gas at high pressure.

The first experiments aiming at understanding the phase behavior and dynamics of dense colloidal suspensions were pioneered by Pusey and van Megen in the 1980s [4, 5]. By performing extensive dynamic light scattering (DLS) measurements, these authors demonstrated that the particles' packing fraction η is the only parameter needed to describe the isotropic-to-crystal-to-glass transitions of hard colloidal spheres [4]. The dynamical behavior is also deeply influenced by η: while in the very dilute regime hard spheres follow an essentially Brownian diffusion, at a denser packing the cage effect exerted by the neighbouring particles determine a transient subdiffusive regime delaying the structural relaxation of the system and the decay of the autocorrelation functions measured by DLS [5]. Since these pioneering results, the interest in the phase behavior and dynamics of dense colloidal suspensions has been growing dramatically and now involves a vibrant area of research including both equilibrium (e.g., liquid crystals) and out-of-equilibrium (e.g., gels and glasses) colloidal suspensions of anisotropic particles [6, 7].

Due to the advances in computational techniques, molecular simulation has played a key role in both supporting (sometimes anticipating) the experimental findings and validating theories. In this respect, the last

* Electronic mail: alessandro.patti@manchester.ac.uk

few years have witnessed a marked interest in investigating the dynamics in dense colloidal suspensions by using simple, but efficient simulation techniques. Although Molecular Dynamics (MD) would perfectly describe the dynamics of a colloidal system, explicitly modelling the solvent, and hence including the degrees of freedom associated to its molecules, would be too computationally demanding. Brownian Dynamics (BD) circumvents this obstacle by implicitly representing the solvent via effective frictional and thermal forces acting on the colloidal particles [8]. At equilibrium, the balance between these forces ensures the correct equilibrium distribution of the system, as stated by the fluctuation/dissipation theorem [9]. Therefore, while care should be taken in selecting relatively small timesteps to accurately integrate the equations of motion, this poses a limit in the evaluation of dynamical properties with long-time decays.

Given the stochastic nature of Brownian motion, dynamic Monte Carlo (DMC) simulation was shown to be an excellent tool to describe the dynamics of colloidal suspensions, especially those characterized by rather long relaxation times, such as glass-forming systems [10–12], liquid crystalline phases [13, 14], solutions of globular proteins [15, 16], and fluids confined to narrow channels [17]. Several works have been recently published on the use of DMC as an alternative to BD to investigate the dynamics of dense suspensions of spherical and anisotropic colloidal particles [18–21]. In all these studies, the authors found a very good agreement between BD and DMC simulations, especially when the elementary displacements and rotations performed by the particles are relatively small. Despite their remarkable results, which allow one to employ standard Metropolis-based MC algorithms to investigate dynamical properties, all these studies focussed on monodisperse systems. In a more general scenario with size and/or shape polydispersity playing a role, for instance to prevent crystallization at high densities [22], different (species of) particles are expected to possess different mobility or, equivalently, to displace different distances in the same unit of time. More specifically, as stated by the Einstein relations, an elementary (translational or rotational) move is linked to the unit timestep via the particle's diffusion coefficient [23], which in turn is a function of the particle's geometry [24, 25]. We stress that this fundamental constraint guarantees a homogeneous time evolution for all the particles, regardless their size and shape, and must be taken into account when modelling bidisperse or, more generally, polydisperse colloidal suspensions by DMC simulation.

Motivated by the remarkable interest of both academy and industry in the dynamics of dense colloidal systems and by the necessity of providing efficient simulation tools to handle the long time scales involved, here we present a theoretical formalism to investigate the dynamics of multicomponent colloidal suspensions by DMC simulations. The theory is validated by studying the dynamical behavior of binary mixtures of rod-like and spherical particles with BD and DMC simulations.

B. Theory

In the following, we extend the theoretical formalism outlined in [20] for monodisperse systems to multicomponent colloidal suspensions containing n_c species. The total number of particles in our system reads

$$N_p = \sum_{j=1}^{n_c} N_j, \tag{1}$$

with N_j the number of particles of species j. By following a standard Metropolis-based MC algorithm, a particle is selected at random (regardless the species it belongs to and the relative concentrations of the species) and moved to a new position with acceptance probability $\exp(-\Delta U/k_BT)$, with ΔU the energy change between the new and old configurations.

More specifically, here we define an MC step as an attempt of simultaneously changing the degrees of freedom of a randomly selected particle. In a three-dimensional space, the number of degrees of freedom is three for spherical particles and five for particles with axial symmetry, three being associated with the displacement of their center of mass and two with their rotation. In the most general case of f degrees of freedom, a particle of species j moves in an f-dimensional hyperprism of volume $V_j = \prod_{k=1}^{f}(2\delta\xi_{k,j})$ centered in its original position, with each degree of freedom changing in the interval $[-\delta\xi_{k,j}, \delta\xi_{k,j}]$. Therefore, an MC step consists of simultaneously changing all the f degrees of freedom of a randomly selected particle. This trial change is eventually accepted with probability $\mathcal{A}_j = \exp(-\Delta U/k_BT)$. In particular, the normalized probability $P^{(n)}_{move,j}$ of successfully moving a particle $n \in j$ in an MC step is the product of the probabilities of (i) selecting a particle n, (ii) moving n in a region of the hyperprism V_j, and (iii) accepting the move:

$$P^{(n)}_{move,j} = \left(\frac{1}{N_p}\right)\left(\frac{1}{V_j}\right)\mathcal{A}_j = \frac{1}{N_p}\frac{\mathcal{A}_j}{V_j}, \forall n \in j \tag{2}$$

We assume $\mathcal{A}_j$ to be uniform in the f-dimensional hyperprism where each degree of freedom is allowed to oscillate between $-\delta\xi_{k,j}$ and $\delta\xi_{k,j}$. This assumption is exact only at infinite dilution or at infinitesimally small $\delta\xi_{k,j}$, where the collisions between particles do not determine significant fluctuations of the acceptance rate. In other words, $\mathcal{A}_j$ is the same for all particles $n \in j$. Under these conditions, the probability to move each of the N_p particles in an MC cycle, being a cycle equal to N_p statistically independent MC steps, reads:

$$P_{move,j} = \sum_{n=1}^{N_p} \frac{1}{N_p}\frac{\mathcal{A}_j}{V_j} = \frac{\mathcal{A}_j}{V_j} \tag{3}$$

To relate the change of position and orientation of a particle to a consistent temporal scale, we employ the Einstein relations or, equivalently, the Langevin equations at long times [23]. Assuming that the MC steps are statistically independent, time and space are related through the self-diffusion coefficients as follows:

$$\delta\xi^2_{k,j} = 2D_{k,j}\delta t_{MC,j}, \tag{4}$$

where $D_{k,j}$ is the self-diffusion coefficient associated to the kth degree of freedom and $\delta t_{MC,j}$ is the timestep in the MC timescale. Both the self-diffusion coefficient and elementary MC timestep are characteristic of the species and basically depend on the particles' geometry. To correlate these observations, we introduce the mean square change of the kth degree of freedom for particles of specie j in an MC cycle:

$$\langle\xi^2_{k,j}\rangle = \int_{V_j} \xi^2_{k,j} P_{move,j} d\xi_{k,j} = \frac{\mathcal{A}_j \delta\xi^2_{k,j}}{3} \tag{5}$$

We highlight that Eq. (5) is strictly valid only if the acceptance rates $\mathcal{A}_j$ can be considered uniform in the f-dimensional hyperprism. The main advantage of DMC over BD is the possibility of exploring longer time scales by increasing the elementary timesteps. Clearly, a larger elementary MC timestep or, equivalently, larger displacements and rotations, would provide lower acceptance rates and delay the dynamical evolution of the system. The compromise between elementary steps and acceptance rates is a known aspect in MC simulations [8]. However, what one should note here is that increasing the elementary MC timesteps would lead to a larger f-dimensional hyperprism, which defines the extension of displacements and rotations of a particle. If the hyperprism becomes too large, the acceptance rates might no longer be considered uniform and Eq. (5) might not be valid. This is a limit of application of the present theory, especially involving highly heterogeneous systems, such as gels or glasses, for which a dependence of the acceptance rates on space and time should be considered.

Eq. (5) can be extended to the case of $N_p = \sum N_j$ particles performing $\mathcal{C}_{MC}$ cycles:

$$\langle\xi^2_{k,j}\rangle = \mathcal{C}_{MC}\frac{\mathcal{A}_j \delta\xi^2_{k,j}}{3} \tag{6}$$

By combining Eq. (6) with Eq. (4), the following result is obtained:

$$\langle\xi^2_{k,j}\rangle = \frac{2}{3}\mathcal{C}_{MC}\mathcal{A}_j D_{k,j}\delta t_{MC,j} \tag{7}$$

Similarly, the Einstein relation for a BD simulation reads

$$\langle\xi^2_{k,j}\rangle = 2D_{k,j}t_{BD} \tag{8}$$

where t_{BD} is the time unit of a BD simulation. Thus, for each species j in the system, in the limit of small $\delta t_{MC,j}$ and uniform $\mathcal{A}_j$ in the f-dimensional hyperprism, a relation between MC and BD timescales is obtained:

$$t_{BD} = \mathcal{C}_{MC}\delta t_{BD} = \frac{\mathcal{A}_j}{3}\mathcal{C}_{MC}\delta t_{MC,j} \tag{9}$$

where δt_{BD} is the elementary timestep in the BD timescale. The practical importance of this result, which also represents the main advance with respect to the formalism presented in [20], is that each species of a multicomponent system possesses an identical BD timestep, but its own MC timestep. Therefore, generalizing the above result to a multicomponent colloidal suspension of n_c different species, we obtain the following relation:

$$\mathcal{A}_1\delta t_{MC,1} = \mathcal{A}_2\delta t_{MC,2} = ... = \mathcal{A}_{n_c}\delta t_{MC,n_c} \tag{10}$$

Eqs. (9) and (10) can be easily extended to polydisperse multicomponent colloidal systems containing particles of different sizes. In this case, j would represent a family of equally sized particles.

C. Model and Simulation Methodology

To validate our theoretical formalism, we performed BD and DMC simulations of bidisperse colloidal suspensions containing $N_p = 1000$ rod-like and spherical colloidal particles in a cubic box. The number of rods is $N_r = 300$, 500 or 700, while the number of spheres is $N_s = N_p - N_r$. Rods are modelled as prolate spherocylinders with aspect ratio $L^* = L/\sigma = 5$, with L and σ the length and diameter, respectively, of a cylinder capped by two hemispheres with diameter σ. The diameter of the spheres is also σ. All particles are represented as soft purely repulsive bodies and interact via a shifted and truncated Kihara potential (SRS):

$$U_{ij} = \begin{cases} 4\epsilon\left[\left(\frac{\sigma}{d_m}\right)^{12} - \left(\frac{\sigma}{d_m}\right)^{6} + \frac{1}{4}\right] & d_m \leq \sqrt[6]{2}\sigma \\ 0 & d_m > \sqrt[6]{2}\sigma \end{cases} \tag{11}$$

U_{ij} is the interaction potential between two generic particles of species i and j (spheres or rods), ϵ the strength of their interaction (the same for sphere-sphere, rod-rod and sphere-rod pairs) and d_m the minimum distance between them. σ, ϵ and $\tau = \sigma^2/D_0$ are the length, energy, and time units, respectively, with $D_0 = k_BT/(\mu\sigma)$ a diffusion constant and μ the viscosity coefficient of the solvent [26]. The interested reader is referred to Refs. [27, 28] for more details on the SRS potential and to Ref. [29] for more details on the computation of the minimum distance d_m between two prolate spherocylinders.

To equilibrate the systems, we performed standard MC simulations in the NPT ensemble at $1 \leq P^* = P\sigma^3/\epsilon \leq 3$

and $T^* = k_B T/\epsilon = 1.465$. At this temperature, the phase behavior of soft spherocylinders resembles that of hard spherocylinders of the same length and diameter [27, 28]. The systems were considered at equilibrium when the total energy, U/ϵ, packing fraction, η, and nematic order parameter achieved a steady value within the statistical fluctuations. Isotropic (I), nematic (Nm) and smectic (Sm) phases have been found and their dynamics studied by BD and DMC simulations. Details on BD simulations for this particular system are given in [30]. Here we only point out that the integration timestep has been set to $\delta t_{BD}/\tau = 10^{-4}$ in all BD simulations.

DMC simulations have been carried out in the NVT ensemble in cuboidal simulation boxes with periodic boundaries. The total number of MC cycles is kept constant to $\mathcal{C}_{MC} = 8 \cdot 10^6$ for all the DMC simulations. Displacements and rotations (the latter only for rods) have been attempted simultaneously and eventually accepted according to the standard Metropolis algorithm. Although this choice does not ensure the detailed-balance condition, it still results in a correct MC sampling. In particular, it has been shown that for an MC algorithm to be valid, the detailed balance is sufficient but not necessary [31]. A sufficient and necessary condition, usually referred to as a simple balance condition, provides a correct criterion to check the effectiveness of an MC scheme. Our DMC algorithm satisfies this condition, as we proved in Ref. [20].

To properly mimic the Brownian dynamics of colloidal suspensions, the DMC trajectory do not involve unphysical moves, such as swaps, jumps or cluster moves. The displacement of spherical particles is decoupled along the three directions of the simulation box: $\delta \mathbf{r}_s = X_x \hat{\mathbf{x}} + X_y \hat{\mathbf{y}} + X_z \hat{\mathbf{z}}$. X_x, X_y and X_z are random numbers fulfilling the condition $|X_l| \leq \delta r_s^{max}$, with $l = x, y, z$ and δr_s^{max} the maximum displacement of a spherical particle along a direction l. Similarly, the displacement of rod-like particles is decoupled as follows: $\delta \mathbf{r}_r = X_{||} \hat{\mathbf{u}}_r + X_{\perp,1} \hat{\mathbf{v}}_{r,1} + X_{\perp,2}\ \hat{\mathbf{v}}_{r,2}$, where $\hat{\mathbf{u}}_r$ is the rod's orientation vector and $\hat{\mathbf{v}}_{r,m}$, with $m = 1$ or 2, are two randomly chosen unit vectors perpendicular to each other and to $\hat{\mathbf{u}}_r$. In each direction, the magnitude of the displacement is chosen at random with the conditions $|X_{||}| \leq \delta r_{||}^{max}$ and $|X_{\perp,m}| \leq \delta r_{\perp}^{max}$, with $\delta r_{||}^{max}$ and $\delta r_{\perp}^{max}$ the maximum elementary displacements in the direction parallel and perpendicular to $\hat{\mathbf{u}}_r$, respectively. Upon rotation, the rod's orientation vector changes from $\hat{\mathbf{u}}_r$ to $\hat{\mathbf{u}}_r + \delta \hat{\mathbf{u}}_r$ with $\delta \hat{\mathbf{u}}_r = Y_{\vartheta,1}\ \hat{\mathbf{w}}_{r,1} + Y_{\vartheta,2}\ \hat{\mathbf{w}}_{r,2}$. In particular, $\hat{\mathbf{w}}_{r,m}$ are two randomly chosen vectors perpendicular to each other and to $\hat{\mathbf{u}}_r$. The random numbers $Y_{\vartheta,m}$ must satisfy the condition $|Y_{\vartheta,m}| \leq \delta \vartheta^{max}$, where $\delta \vartheta^{max}$ is the maximum elementary rotation of the main axis of the rods. The maximum displacements and rotations can be calculated by applying the Einstein relations given in Eq. (4):

$$\delta r_s^{max} = \sqrt{2 D_s \delta t_{MC,s}}, \tag{12}$$

$$\delta r_{\perp}^{max} = \sqrt{2 D_{r,\perp} \delta t_{MC,r}}, \tag{13}$$

$$\delta r_{\parallel}^{max} = \sqrt{2 D_{r,\parallel} \delta t_{MC,r}}, \tag{14}$$

$$\delta \vartheta^{max} = \sqrt{2 D_{r,\vartheta} \delta t_{MC,r}} \tag{15}$$

The self-diffusion coefficient of spherical particles is given by the Stokes-Einstein equation:

$$D_s/D_0 = \frac{1}{3\pi} \tag{16}$$

By contrast, the rod's self-diffusion coefficients are obtained from the analytical expressions available for prolate spheroids [24, 25]:

$$D_{r,\perp}/D_0 = \frac{(2a^2 - 3b^2)S + 2a}{16\pi(a^2 - b^2)} b, \tag{17}$$

$$D_{r,\parallel}/D_0 = \frac{(2a^2 - b^2)S - 2a}{8\pi(a^2 - b^2)} b, \tag{18}$$

$$D_{r,\vartheta}/D_0 = 3\frac{(2a^2 - b^2)S - 2a}{16\pi(a^4 - b^4)} b. \tag{19}$$

where $a = (L + \sigma)/2$, $b = \sigma/2$, and S is a geometrical parameter given by

$$S = \frac{2}{(a^2 - b^2)^{1/2}} \log \frac{a + (a^2 - b^2)^{1/2}}{b}. \tag{20}$$

The complete set of values of the four above self-diffusion coefficients is given in Table I.

TABLE I. Self-diffusion coefficients of rods, with length-to-diameter ratio $L/\sigma = 5$, and spheres, with diameter σ, as calculated from Eqs. (16-19).

D_s/D_0	$D_{r,\perp}/D_0$	$D_{r,\parallel}/D_0$	$D_{r,\vartheta}/D_0$
$1.554 \cdot 10^{-1}$	$5.812 \cdot 10^{-2}$	$7.907 \cdot 10^{-2}$	$1.282 \cdot 10^{-2}$

The maximum elementary rotations and displacements are set by the DMC timesteps, $\delta t_{MC,s}$ and $\delta t_{MC,r}$. As stated in Eq. (10), the timestep of rods and spheres are related via their respective acceptance rates that are not known *a priori*. One of the two timesteps can be set independently, while the other is updated via a preliminary trial-and-error DMC run preceding the DMC production run. In particular, the time of the slowest species, $\delta t_{MC,r}$, is set and kept constant to $10^{-4}\tau$, $10^{-3}\tau$

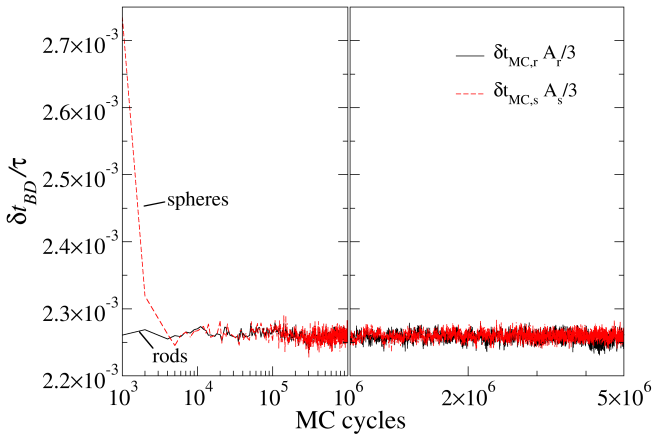

FIG. 1. (Color online). Convergence of the elementary MC timestep $\delta t_{MC,s}$ to $\delta t_{MC,r}\mathcal{A}_r/\mathcal{A}_s$, rescaled according to Eq. (10), during the preliminary trial-and-error procedure (left frame). The two rescaled elementary timesteps achieve a steady value very quickly and mantain it, within the statistical fluctuations, along the production run (right frame).

or $10^{-2}\tau$, while $\delta t_{MC,s}$ is allowed to converge to its final value according to the instantaneous acceptance rates of spheres and rods. More specifically, $\delta t_{MC,s}$ is initially set equal to $\delta t_{MC,r}$ and recalculated at the end of every MC cycle to satisfy the constraint of Eq. (10), that is $\delta t_{MC,s} = \delta t_{MC,r}\mathcal{A}_r/\mathcal{A}_s$. With this updated elementary timestep, the maximum displacement for spheres is recalculated from Eq. (12) and a new value of $\mathcal{A}_s$ generated. This preliminary trial-and-error algorithm converges very fast, as can be appreciated in Fig. 1, which shows the typical convergence of the elementary MC timestep $\delta t_{MC,s}$ to $\delta t_{MC,r}\mathcal{A}_r/\mathcal{A}_s$ for the systems studied here. The steady value of $\delta t_{MC,s}$ is then used in the production run to calculate the dynamical properties of the colloidal particles. In the production run, the elementary MC timesteps are kept constant, but the acceptance rates can fluctuate around an average value whose standard deviation, basically depending on the packing of the system, is relatively small and generally in the order of 10^{-4}. Standard deviations are useful to quickly estimate the magnitude of fluctuations of the acceptance rates and thus to justify the validity of Eq. (5).

To quantitatively compare the results from DMC and BD simulations and thus address the validity of Eqs. (9) and (10), we have calculated the mean square displacements (MSDs), the orientation auto-correlation functions (OAFs) and the self part of the van Hove correlation functions (s-VHFs) of several systems at different compositions, packing fractions and timesteps. These functions have been averaged out over trajectories with multiple time origins to collect good statistics. The MSD, calculated separately for spheres and rods, results from the displacements along the three axes of the simulation box and reads:

$$\langle \Delta r_j^2(t) \rangle = \frac{1}{N_j} \left\langle \sum_{n=1}^{N_j} \left(\mathbf{r}_{n,j}(t) - \mathbf{r}_{n,j}(0) \right)^2 \right\rangle , \qquad (21)$$

where the delimiters $\langle ... \rangle$ denote ensemble average. In case of systems forming nematic or smectic phases, the MSD of rods and spheres can be decoupled in the direction parallel, $\langle \Delta r_{j,\parallel}^2(t) \rangle$, and perpendicular, $\langle \Delta r_{j,\perp}^2(t) \rangle$, to the nematic director $\hat{\mathbf{n}}$ of the liquid crystalline phase. The OAF, limited to the rod-like particles, is given by the second Legendre polynomial of the dot product between the unit orientation vectors, $\hat{\mathbf{u}}_{n,r}(0)$ and $\hat{\mathbf{u}}_{n,r}(t)$, of a particle n calculated at time 0 and time t, respectively:

$$E_2(t) = \frac{1}{N_r} \left\langle \sum_{n=1}^{N_r} \frac{1}{2} \left\{ 3 \left[\hat{\mathbf{u}}_{n,r}(0) \cdot \hat{\mathbf{u}}_{n,r}(t) \right]^2 - 1 \right\} \right\rangle \qquad (22)$$

Finally, the distribution of displacements can be quantitatively described by the s-VHFs that measure the probability distribution for a particle displacement $\mathbf{r}$ after an interval of time t. We separately estimate the s-VHF in the direction parallel and perpendicular to the nematic director by evaluating the following functions:

$$G_s^{\parallel}(r_{\parallel}, t) = \frac{1}{N} \langle \sum_{j=1}^{N} \delta(\mathbf{r}_{\parallel} - \mathbf{r}_{\parallel,j}(t+t_0) + \mathbf{r}_{\parallel,j}(t_0)) \rangle \qquad (23)$$

$$G_s^{\perp}(r_{\perp}, t) = \frac{1}{N} \langle \sum_{j=1}^{N} \delta(\mathbf{r}_{\perp} - \mathbf{r}_{\perp,j}(t+t_0) + \mathbf{r}_{\perp,j}(t_0)) \rangle_{2\pi} \qquad (24)$$

with $(\mathbf{r}_{\perp,j}(t), \mathbf{r}_{\parallel,j}(t))$ the location of particle j at time t, δ the Dirac-delta, $\langle ... \rangle$ the ensemble average. The index 2π indicates the average over the polar angle which defines the bidimensional vector $\mathbf{r}_{\perp}$. It should be noticed that for freely diffusive particles these functions are described by a Gaussian.

D. Results

To validate our theoretical formalism, we investigate the dynamical behavior of a bidisperse colloidal mixture of rods and spheres at three different concentrations. In particular, $N_r/N_p = 0.3$, 0.5 and 0.7. These systems are able to form *I*, *Nm* and *Sm* phases as exemplarily shown in Fig. 2. The *I* phase does not exhibit any appreciable long-range order as both components distribute randomly in the space. At higher pressure, the *I* phase transforms into the *Nm* phase, where the rods are preferentially oriented along a common nematic director, $\hat{\mathbf{n}}$, while the spheres maintain a rather weakly ordered distribution. In the *Sm* phase, both components display an evident translational long-range order in the direction

of the nematic director with the rods forming oriented lamellar stacks that drive the distribution of the spherical particles, mostly located in the inter-layer region. Details of the systems studied in this work are summarized in Table II.

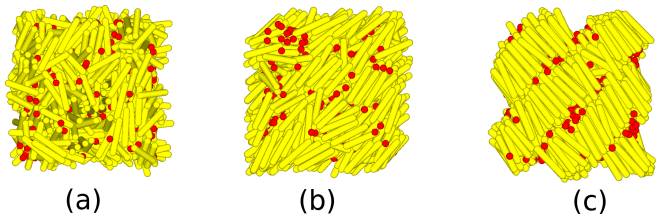

FIG. 2. Isotropic (a), nematic (b), and smectic (c) phases containing 70% rods with length-to-diameter ratio $L/\sigma = 5$ and 30% spheres with diameter σ. The three phases are at the same temperature $T^* = 1.465$ and packing fraction η =0.409 (a), 0.467 (b) and 0.524 (c).

To illustrate how the DMC results are practically rescaled to the BD results, the MSDs of 300 spheres and 700 rods forming an isotropic phase at $P^* = 1$ are analyzed in Fig. 3. The MSDs as calculated by DMC simulations are represented by dashed lines, whereas the open symbols reproduce the results of BD simulations. In both cases, the MSDs are those typical of a dilute colloidal suspension following a liquid-like dynamics. The dashed curves are obtained at an arbitrarily set MC timestep for rods, which is $\delta t_{MC,r}/\tau = 10^{-4}$ in this case, while the MC timestep for spheres, $\delta t_{MC,s}/\tau = 9.9 \cdot 10^{-5}$, results from convergence of Eq. (10) along a short preliminary DMC simulation implementing the trial-and-error algorithm described above. At these timesteps, the acceptance rates estimated at the end of the production run are $\mathcal{A}_r = 0.981$ and $\mathcal{A}_s = 0.991$ for rods and spheres, respectively. With these values of acceptance rates and elementary timesteps, we apply Eq. (9) to recover the physical time of the DMC production run and thus the BD timescale. The solid lines shown in Fig. 3, being the rescaled MSDs from the DMC simulations, indicate an excellent quantitative agreement with BD simulations. The inset in Fig. 3 displays the same MSDs in a double linear scale to better appreciate the deviations between BD and rescaled DMC results, being however not particularly significant.

The advantage of DMC over BD simulations is the possibility of addressing the long-time dynamics of dense colloidal systems by increasing the elementary timestep. With the limits imposed by Eq. (5), we have increased $\delta t_{MC,r}$ up to $10^{-2}\tau$. Depending on the packing of the system, at this elementary timestep the acceptance rates decrease up to $\mathcal{A}_r = 0.677$ with standard deviations in the order of 10^{-3} (Sm phase with $N_r = 700$). Nevertheless, we still observe an excellent agreement with BD simulations, as illustrated in Fig. 4, where we show the MSDs of rods and spheres in isotropic phases at three different relative compositions $N_r/N_p = 0.3$ (top), 0.5 (middle) and 0.7 (bottom frame), and three different ele-

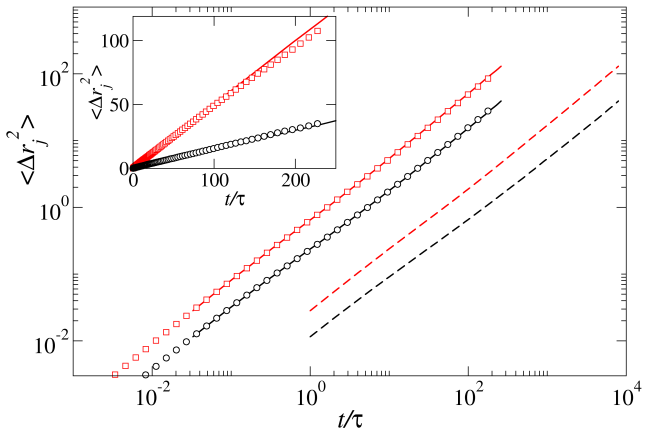

FIG. 3. (Color online) Mean square displacements (MSDs) in an isotropic phase (η =0.409) containing $N_r = 700$ rod-like and $N_s = 300$ spherical particles. Circles and squares indicate the MSD of rods and spheres, respectively, obtained from BD simulations. Black (lower) and red (upper) dashed lines refer to the MSD of rods and spheres, respectively, obtained from DMC simulations at $\delta t_{MC,r} = 10^{-4}\tau$ and $\delta t_{MC,s} = 9.9 \cdot 10^{-5}\tau$ and acceptance rates $\mathcal{A}_r = 0.981$ and $\mathcal{A}_s = 0.991$. The solid lines are the same MSDs from DMC simulations with the time rescaled according to Eq. (9). The inset, in double linear scale, shows the BD and rescaled DMC results.

mentary timesteps. By keeping the total number of MC cycles constant and increasing $\delta t_{MC,r}$ (and consequently $\delta t_{MC,s}$) it is possible to explore the long-time dynamics of our model colloidal suspensions without lack of accuracy with respect to the dynamics described by BD simulations. We note that increasing the relative amount of rods from 30% to 70% has a limited effect on the MSDs shown in Fig. 4, which might be due to the rather dilute concentrations considered in this particular case.

The MSDs of the two species in the Nm and Sm phases are given in Fig. 5. Spherical particles have a similar dynamics in the Nm and Sm phases, although their diffusion in the direction parallel to the nematic director $\hat{\mathbf{n}}$ of the Sm phase appears to be reduced as compared to their parallel diffusion in the Nm phase. The dynamics of rods in the two liquid crystal phases is significantly different and influenced by the layered structure that hampers their diffusion in the direction of $\hat{\mathbf{n}}$ in the Sm phase. In the Nm phase, the parallel MSD is larger than the perpendicular MSD from short to long times, as also found elsewhere [30, 32]. By contrast, in the Sm phase, this behavior is only observed at short times, when the rods are still diffusing in the cage formed by their nearest neighbors. This cage is particularly effective in the direction of $\hat{\mathbf{n}}$ by providing a barrier against the diffusion of the rods [13]. This explains why the slope of $< \Delta r^2_{r,\parallel} >$ decreases at intermediate times and, when the rods enter the diffusive regime, remains rather lower than $< \Delta r^2_{r,\perp} >$. All these details are captured by BD and DMC simulations with excellent agreement, confirming that our algorithm

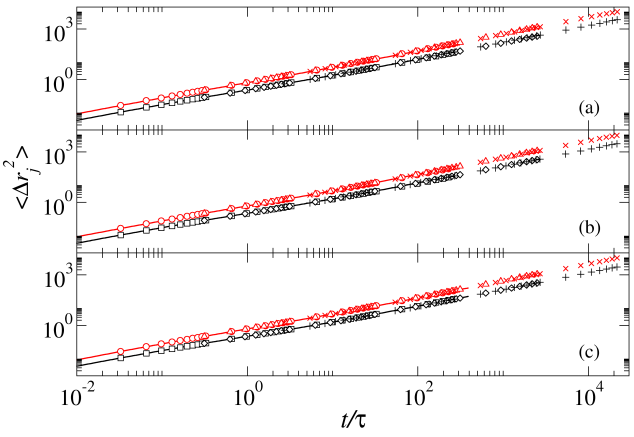

FIG. 4. (Color online) Mean square displacements (MSDs) in isotropic phases containing 30% (a), 50% (b) and 70% (c) of rod-like particles at $T^* = 1.465$ and $P^* = 1$. Black (lower) and red (upper) lines represent the results of BD simulations for rods and spheres, respectively. The symbols indidate the rescaled MSDs for the following rods' elementary MC timesteps: $\delta t_{MC,r} = 10^{-4}\tau$, $\delta t_{MC,r} = 10^{-3}\tau$ and $\delta t_{MC,r} = 10^{-2}\tau$. The respective elementary timesteps for spheres and acceptance rates are given in Table II.

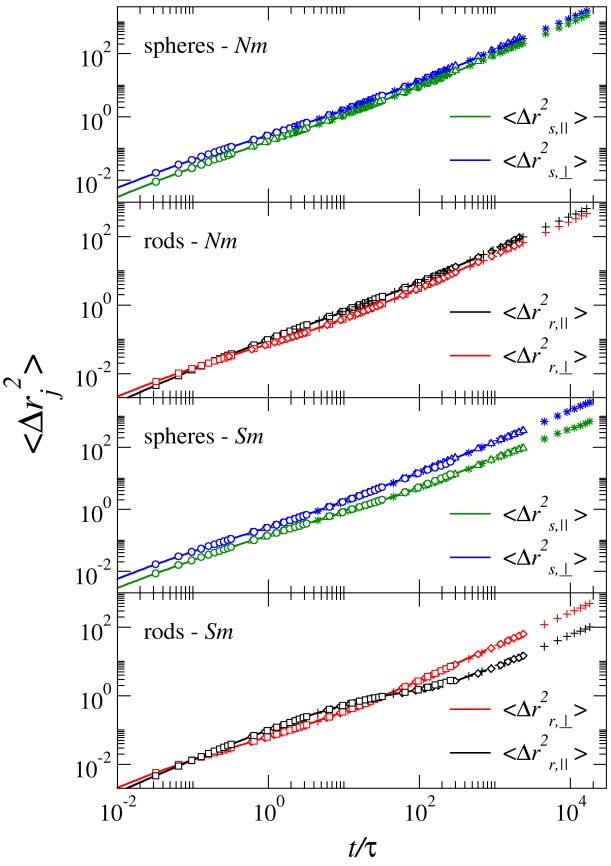

FIG. 5. (Color online) Mean square displacements (MSDs) of spheres and rods in the *Nm* and *Sm* phases containing 70% of rod-like particles at $T^* = 1.465$ and η =0.467 (*Nm*) and 0.524 (*Sm*). The MSDs are shown for both species in the direction parallel and perpendicular to the nematic director. The solid lines refer to BD simulations, while the symbols to DMC simulations at $\delta t_{MC,r}/\tau = 10^{-4}$ ($\square$), 10^{-3} ($\diamond$) and 10^{-2} ($+$) and rescaled according to Eq. (9). The respective acceptance rates and elementary timesteps for spheres (symbols at increasing $\delta t_{MC,s}$: $\bigcirc$, $\triangle$ and $\times$) are given in Table II.

works very well also for multicomponent systems showing a complex dynamics. These results point out an excellent agreement between DMC and BD simulations for species whose dynamical evolution is actually not particularly different. To test whether our theoretical framework is still valid when the dynamics of one of the two species is rather slower than the other, we have also simulated *Sm* phases containing longer rods, with aspect ratio $L^* = 7$, by keeping the spheres' diameter equal to σ. The resulting MSDs are given in Fig. 6. Despite the evident difference of mobility between spheres and rods, especially in the direction parallel to $\hat{\mathbf{n}}$, the agreement between DMC and BD simulations is again excellent, confirming that the applicability of our theoretical framework is not limited to species with a homogeneous dynamics.

In Fig. 7, the orientation auto-correlation functions of rod-like particles, calculated from Eq. (22), are given for the *I*, *Nm* and *Sm* phases. The fast exponential decay of $E_2(t)$ is expected for liquid-like systems, while liquid crystals, due to the quasi-aligned orientation of the rods, exhibit a decay of $E_2(t)$ to a positive value, which is roughly 0.6 in the *Nm* phase and 0.85 in the *Sm* phase. Rescaling the results of DMC simulations gives an excellent agreement with the results of BD simulations for the three phases of interest. A peculiar feature of rods' diffusion in the *Sm* phase is their tendency to rattle around in a given layer until they *jump* to a neighboring layer [13]. A similar behavior has also been observed in binary mixtures of rods and spheres, with the latter preferentially hopping between the interlayer spaces [30]. In Fig. 8, we provide the s-VHFs of rods and spheres in a *Sm* phase containing $N_r = 700$ rods and $N_s = 300$ spheres, with packing fraction $\eta = 0.524$. As expected, the distribution of the displacements in the direction of the nematic director reveals the appearance of secondary peaks at relatively long times and approximately $r = L$. These peaks highlight the presence of preferential displacements along the nematic director for spheres and, especially, for rods. The rescaled s-VHFs obtained from DMC simulations reveal that this tendency is grasped by both DMC and BD simulations with identical precision. The s-VHFs calculated in the *I* and *Nm* phases (not shown here) show also an excellent agreement between DMC and BD simulations.

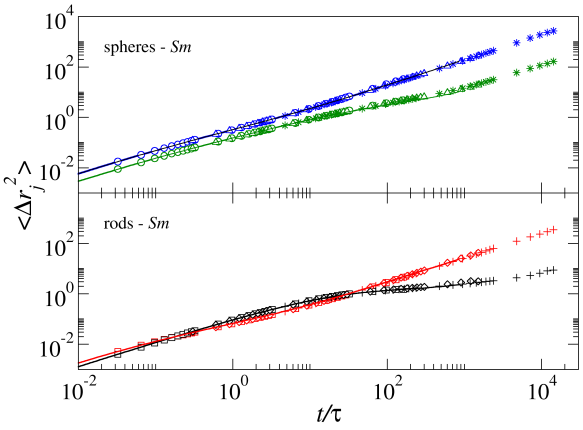

FIG. 6. (Color online). Mean square displacements (MSDs) in a smectic phase (η =0.513) containing 300 spheres and 700 rods with aspect ratio $L^* = 7$. The MSDs are shown for spheres (top frame) and rods (bottom frame) in the direction parallel (lower curves) and perpendicular (upper curves) to the nematic director. The solid lines refer to BD simulations, while the symbols to DMC simulations at $\delta t_{MC,r}/\tau = 10^{-4}$ (□), 10^{-3} (◇) and 10^{-2} (+) and rescaled according to Eq. (9). The respective elementary timesteps for spheres are $\delta t_{MC,s} = 9.843 \cdot 10^{-5}\tau$ (○), $9.480 \cdot 10^{-4}\tau$ (△) and $8.187 \cdot 10^{-3}\tau$ (×).

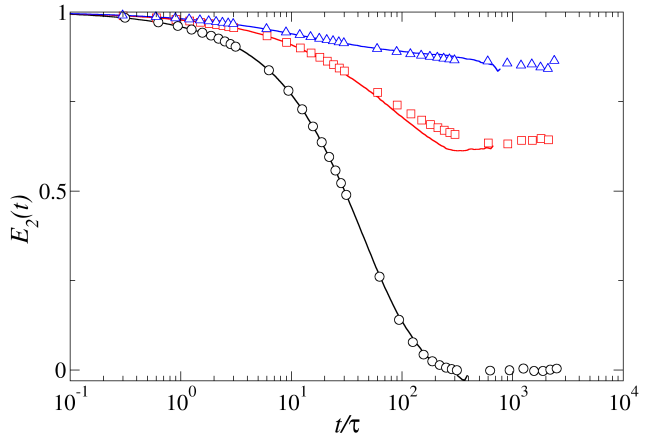

FIG. 7. (Color online) Orientation auto-correlation functions (OAFs), $E_2(t)$, in the isotropic (black ○), nematic (red □), and smectic (blue △) phases of rod-like particles. The solid lines refer to BD simulations, whereas the symbols are the results from DMC simulations with the time rescaled according to Eq. (9). For the three systems, $N_r/N_p = 0.7$ and $\delta t_{MC,r} = 10^{-3}\tau$, whereas η =0.317, 0.467 and 0.524 for the *I*, *Nm* and *Sm* phase, respectively. The respective elementary timesteps for spheres and the acceptance rates are given in Table II.

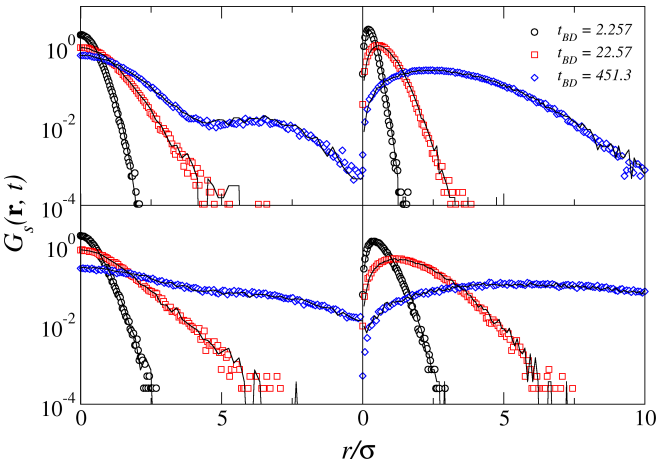

FIG. 8. (Color online). Longitudinal (left) and transverse (right) component of the self-part of the van Hove function of rods (top) and spheres (bottom) in a *Sm* phase containing 70% of rod-like particles at $T^* = 1.465$ and η =0.524. All symbols refer to the results obtained from DMC simulations with the time rescaled according to Eq. (9). The solid lines refer to BD simulations.

E. Conclusions

In summary, we have presented an efficient theoretical framework to investigate the dynamics of multicomponent colloidal suspensions by DMC simulations. To validate our theory, we considered a bidisperse mixture of colloidal rods and spheres, whose dynamical properties have been calculated by performing BD and DMC simulations. Each component has its own elementary timestep which must be carefully set to obtain a consistent and unique MC timescale. We have proposed a simple trial-and-error procedure to compute the elementary timesteps and hence compare the results of DMC and BD simulations.

To accurately describe the Brownian dynamics via DMC simulations, it is crucial to observe that particles of different species do not have the same mobility and do not move the same distances along the same unit of time. In other words, the maximum displacements and rotations allowed in a DMC simulation are different for different components. Nevertheless, we have showed that the elementary timesteps of the species in the system are not independent, but correlated via the acceptance rate of the simultaneous change of all the degrees of freedom involved. In particular, regardless the species j, we found that $\mathcal{A}_j \delta t_{MC,j}/3$ is constant and equals the elementary timestep in the BD timescale. By rescaling the MC timestep with the acceptance rate, the dynamical properties obtained with DMC simulations at different timesteps, collapse into a single master curve, which confirms the existence of a unique MC time scale. The quantitative agreement between the two simulation methods is excellent, but DMC provides the remarkable advantage of approaching longer time scales as compared to BD, whose timestep must be small enough to integrate the stochastic equations of motion accurately.

We highlight that the theoretical formalism presented

here is of general applicability and can be extended to any polydisperse colloidal suspension. It works very well even when the dynamical behaviour of one of the species is rather slow, as in the case of long rods, or characterized by non-uniform distribution of displacements, as generally observed with smectic LCs. This makes DMC simulation a powerful tool to efficiently investigate the long-time dynamics of dense systems. However, we stress that our theoretical approach is strictly applicable under stationary conditions, where the acceptance rate, apart from minor statistical fluctuations, can be considered constant along the DMC production run. This implies that the dependence of the acceptance rate on time and space should be considered when studying heterogeneous systems, such as colloidal gels or glass-forming systems.

F. Acknowledgments

AC acknowledges projects CTQ2012-32345 and P12-FQM-2310 funded by the Spanish Ministry MINECO and by the Junta de Andalucía-FEDER, respectively. AP acknowledges a mobility fellowship offered by the Royal Society of Chemistry (RSC) for funding his research stay at the Department of Physical, Chemical and Natural Systems, Pablo de Olavide University.

[1] G. L. Hunter and E. R. Weeks, Rep. Prog. Phys. **75**, 066501 (2012).
[2] H. N. W. Lekkerkerker and R. Tuinier, *Colloids and the Depletion Interaction*, Lecture Notes in Physics, edited by Springer, Vol. 833 (2011).
[3] R. L. Hoffman, *Trans. Soc. Rheol.* **16**, 155 (1972).
[4] P. N. Pusey and W. van Megen, Nature (London) **320**, 340 (1986).
[5] W. van Megen, R. H. Ottewill, S. M. Owens, and P. N. Pusey, J. Chem. Phys. **82**, 508 (1985).
[6] R. C. Kramb and C. F. Zukoski, J. Rheol. **55**, 1069 (2011).
[7] Y. Joshi, Annu. Rev. Chem. Biomol. Eng. **5**, 181 (2014).
[8] M. Allen and D. Tildesley, *Computer Simulation of Liquids*, edited by Oxford University Press (1987).
[9] J.-L. Barrat and J.-P. Hansen, *Basic concepts for simple and complex liquids*, edited by Cambridge University Press (2003).
[10] L. Berthier and W. Kob, J. Phys.: Condens. Matter **19**, 205130 (2007).
[11] L. Pfleiderer, K. Milinkovic, and T. Schilling, Europhys. Lett. **84**, 16003 (2008).
[12] G. Brambilla, D. El Masri, M. Pierno, L. Berthier, L. Cipelletti, G. Petekidis and A. B. Schofield, Phys. Rev. Lett. **102**, 085703 (2009).
[13] A. Patti, D. El Masri, R. van Roij, and M. Dijkstra, Phys. Rev. Lett. **103**, 248304 (2009).
[14] A. Patti, S. Belli, R. van Roij, and M. Dijkstra, Soft Matter **7**, 3533 (2011).
[15] D. Fusco and P. Charbonneau, Phys. Rev. E **88**, 012721 (2013).
[16] D. Fusco and P. Charbonneau, J. Phys. Chem. B **118**, 8034 (2014).
[17] S. N. Wanasundara, R. J. Spiteri and R. K. Bowles, J. Chem. Phys. **140**, 024505 (2014).
[18] E. Sanz and D. Marenduzzo, J. Chem. Phys. **132**, 194102 (2010).
[19] F. Romano, C. De Michele, D. Marenduzzo, and E. Sanz, J. Chem. Phys. **135**, 124106 (2011).
[20] A. Patti and A. Cuetos, Phys. Rev. E **86**, 011403 (2012).
[21] S. Jabbari-Farouji and E. Trizac, J. Chem. Phys. **137**, 054107 (2012).
[22] P. N. Pusey and W. van Megen, Phys. Rev. Lett. **59**, 2083 (1987).
[23] A. Einstein, *Investigations of the Theory of Brownian Movement* (Dover, New York, 1956).
[24] F. Perrin, J. Phys. Radium **5**, 497 (1934).
[25] H. Shimizu, J. Chem. Phys. **37**, 765 (1962).
[26] H. Löwen, Phys.Rev.E **50**, 1232 (1994).
[27] A. Cuetos, B. Martínez-Haya, S. Lago, and L. F. Rull, J. Phys. Chem. B **109**, 13729 (2005).
[28] A. Cuetos and B. Martínez-Haya, Mol. Phys **113**, 1137 (2015).
[29] C. Vega and S. Lago, Computers & Chemistry **18**, 55 (1994)
[30] M. Piedrahita, A. Cuetos and B. Martínez-Haya, Soft Matter **11**, 3432 (2015).
[31] V. I. Manousiouthakis and M. W. Deem, J. Chem. Phys. **110**, 2753 (1999).
[32] H. Löwen, Phys. Rev. E **59**, 1989 (1999).

TABLE II. Details of the systems studied in this paper, consisting of rods with length to diameter ratio $L^* = L/\sigma$ and spheres with diameter σ. For comparison, we report the reduced pressure P^*, packing fraction $\eta = (N_s v_s + N_r v_r)/V$ with v_j the single particle volume, phase order, relative amount of rods, elementary timesteps $\delta t_{MC,r}$ and $\delta t_{MC,s}$, maximum displacements δr_s^{max}, $\delta r_\parallel^{max}$ and $\delta r_\perp^{max}$, maximum rotation δr_ϑ^{max}, and acceptance rates $\mathcal{A}_r$ and $\mathcal{A}_s$.

P^*	η	Phase	N_r/N_p	$\delta t_{MC,r}/\tau$	$\delta t_{MC,s}/\tau$	$\delta r_s^{max}/\sigma$	$\delta r_\parallel^{max}/\sigma$	$\delta r_\perp^{max}/\sigma$	$\delta\vartheta^{max}$	$\mathcal{A}_r$	$\mathcal{A}_s$
1	0.276	I	0.3	10^{-4}	$9.900{\cdot}10^{-5}$	$1.110{\cdot}10^{-2}$	$7.953{\cdot}10^{-3}$	$6.819{\cdot}10^{-3}$	$3.203{\cdot}10^{-3}$	0.982	0.991
1	0.276	I	0.3	10^{-3}	$9.682{\cdot}10^{-4}$	$3.470{\cdot}10^{-2}$	$2.515{\cdot}10^{-2}$	$2.156{\cdot}10^{-2}$	$1.013{\cdot}10^{-2}$	0.941	0.972
1	0.276	I	0.3	10^{-2}	$8.923{\cdot}10^{-3}$	$1.053{\cdot}10^{-1}$	$7.953{\cdot}10^{-2}$	$6.819{\cdot}10^{-2}$	$3.203{\cdot}10^{-2}$	0.818	0.917
1	0.305	I	0.5	10^{-4}	$9.900{\cdot}10^{-5}$	$1.110{\cdot}10^{-2}$	$7.953{\cdot}10^{-3}$	$6.819{\cdot}10^{-3}$	$3.203{\cdot}10^{-3}$	0.981	0.991
1	0.305	I	0.5	10^{-3}	$9.677{\cdot}10^{-4}$	$3.469{\cdot}10^{-2}$	$2.515{\cdot}10^{-2}$	$2.156{\cdot}10^{-2}$	$1.013{\cdot}10^{-2}$	0.940	0.971
1	0.305	I	0.5	10^{-2}	$8.901{\cdot}10^{-3}$	$1.052{\cdot}10^{-1}$	$7.953{\cdot}10^{-2}$	$6.819{\cdot}10^{-2}$	$3.203{\cdot}10^{-2}$	0.812	0.913
1	0.317	I	0.7	10^{-4}	$9.900{\cdot}10^{-5}$	$1.110{\cdot}10^{-2}$	$7.953{\cdot}10^{-3}$	$6.819{\cdot}10^{-3}$	$3.203{\cdot}10^{-3}$	0.981	0.991
1	0.317	I	0.7	10^{-3}	$9.684{\cdot}10^{-4}$	$3.470{\cdot}10^{-2}$	$2.515{\cdot}10^{-2}$	$2.156{\cdot}10^{-2}$	$1.013{\cdot}10^{-2}$	0.940	0.971
1	0.317	I	0.7	10^{-2}	$8.927{\cdot}10^{-3}$	$1.054{\cdot}10^{-1}$	$7.953{\cdot}10^{-2}$	$6.819{\cdot}10^{-2}$	$3.203{\cdot}10^{-2}$	0.814	0.912
2	0.360	I	0.3	10^{-4}	$9.866{\cdot}10^{-5}$	$1.108{\cdot}10^{-2}$	$7.953{\cdot}10^{-3}$	$6.819{\cdot}10^{-3}$	$3.203{\cdot}10^{-3}$	0.973	0.986
2	0.360	I	0.3	10^{-3}	$9.561{\cdot}10^{-4}$	$3.448{\cdot}10^{-2}$	$2.515{\cdot}10^{-2}$	$2.156{\cdot}10^{-2}$	$1.013{\cdot}10^{-2}$	0.916	0.958
2	0.360	I	0.3	10^{-2}	$8.451{\cdot}10^{-3}$	$1.025{\cdot}10^{-1}$	$7.953{\cdot}10^{-2}$	$6.819{\cdot}10^{-2}$	$3.203{\cdot}10^{-2}$	0.740	0.876
2	0.386	I	0.5	10^{-4}	$9.871{\cdot}10^{-5}$	$1.108{\cdot}10^{-2}$	$7.953{\cdot}10^{-3}$	$6.819{\cdot}10^{-3}$	$3.203{\cdot}10^{-3}$	0.973	0.986
2	0.386	I	0.5	10^{-3}	$9.570{\cdot}10^{-4}$	$3.450{\cdot}10^{-2}$	$2.515{\cdot}10^{-2}$	$2.156{\cdot}10^{-2}$	$1.013{\cdot}10^{-2}$	0.916	0.958
2	0.386	I	0.5	10^{-2}	$8.480{\cdot}10^{-3}$	$1.027{\cdot}10^{-1}$	$7.953{\cdot}10^{-2}$	$6.819{\cdot}10^{-2}$	$3.203{\cdot}10^{-2}$	0.742	0.875
2	0.409	I	0.7	10^{-4}	$9.869{\cdot}10^{-5}$	$1.108{\cdot}10^{-2}$	$7.953{\cdot}10^{-3}$	$6.819{\cdot}10^{-3}$	$3.203{\cdot}10^{-3}$	0.973	0.986
2	0.409	I	0.7	10^{-3}	$9.570{\cdot}10^{-4}$	$3.450{\cdot}10^{-2}$	$2.515{\cdot}10^{-2}$	$2.156{\cdot}10^{-2}$	$1.013{\cdot}10^{-2}$	0.916	0.957
2	0.409	I	0.7	10^{-2}	$8.499{\cdot}10^{-3}$	$1.028{\cdot}10^{-1}$	$7.953{\cdot}10^{-2}$	$6.819{\cdot}10^{-2}$	$3.203{\cdot}10^{-2}$	0.741	0.872
2.5	0.467	Nm	0.7	10^{-4}	$9.854{\cdot}10^{-4}$	$1.107{\cdot}10^{-2}$	$7.953{\cdot}10^{-3}$	$6.819{\cdot}10^{-3}$	$3.203{\cdot}10^{-3}$	0.970	0.984
2.5	0.467	Nm	0.7	10^{-3}	$9.515{\cdot}10^{-4}$	$3.440{\cdot}10^{-2}$	$2.515{\cdot}10^{-2}$	$2.156{\cdot}10^{-2}$	$1.013{\cdot}10^{-2}$	0.904	0.949
2.5	0.467	Nm	0.7	10^{-2}	$8.287{\cdot}10^{-3}$	$1.015{\cdot}10^{-1}$	$7.953{\cdot}10^{-2}$	$6.819{\cdot}10^{-2}$	$3.203{\cdot}10^{-2}$	0.707	0.852
3	0.524	Sm	0.7	10^{-4}	$9.842{\cdot}10^{-5}$	$1.106{\cdot}10^{-2}$	$7.953{\cdot}10^{-3}$	$6.819{\cdot}10^{-3}$	$3.203{\cdot}10^{-3}$	0.966	0.982
3	0.524	Sm	0.7	10^{-3}	$9.473{\cdot}10^{-4}$	$3.432{\cdot}10^{-2}$	$2.515{\cdot}10^{-2}$	$2.156{\cdot}10^{-2}$	$1.013{\cdot}10^{-2}$	0.894	0.944
3	0.524	Sm	0.7	10^{-2}	$8.084{\cdot}10^{-3}$	$1.003{\cdot}10^{-1}$	$7.953{\cdot}10^{-2}$	$6.819{\cdot}10^{-2}$	$3.203{\cdot}10^{-2}$	0.677	0.838